Optica Applicata, Vol. XIX, No. 1, 1989

Zn_3P_2-based solar cell devices

J. M. Pawlikowski

Institute of Physics, Technical University of Wrocław, Wybrzeże Wyspiańskiego 27, 50-370 Wrocław, Poland.

A retrospective survey of the current status of Zn_3P_2-based solar cells is presented. The paper includes a short review of the fundamental properties of Zn_3P_2, the discussion of some technological problems in the devices and the theoretical estimations of the parameters of Zn_3P_2-based solar cells. Finally, the best achievements in the prototype devices area are thoroughly considered, comprising the opaque-metal-grid and transparent-metal-film Schottky-type devices and the Zn_3P_2-based heterojunction-type ones.

1. Introduction

Zinc phosphide (Zn_3P_2) has become one of the promising semiconductors as the absorbing-generating material for applications in photovoltaic solar energy conversion. Both the values of the direct energy bandgap and the diffusion length of minority carriers (see below) promote reasonably high energy conversion efficiency. Furthermore, both Zn and P are abundant and relatively inexpensive, which is perhaps even the equally important feature. Prototype Zn_3P_2-based solar cell devices have been recently fabricated and tested, strengthening a need to promote further investigations of both the fundamental properties of Zn_3P_2 and the electronic performance of Zn_3P_2-based devices.

The successful development of any photoelectric device can be traced through a number of distinct stages. The first step is to identify a semiconductor for potentially effective application in photoconversion systems. To identify such a semiconductor means to find out the energy location and shape of the fundamental absorption edge; to estimate minority carrier diffusion length and material resistivity; to establish the thermal and chemical stabilities of the semiconductor and device; and, finally, to figure out the mineralogical abundance of constituents and cost of their extraction and refinement. Following that there come studies of photon collection efficiency (PCE), quantum efficiency of photo-generation processes (QE), carrier collection efficiency (CCE), and then parameters of prototype devices at various configurations. The next stage is the production and development of the prototype devices leading finally to a large-scale production technology. Considering the development of the Zn_3P_2-based solar cells, both the first and the second stages have been successfully completed.

It is a goal of this paper to discuss shortly the basic properties of Zn_3P_2 and to present the current status of the Zn_3P_2-based prototype devices for broad-range photoconverter applications.

2. Optical properties of Zn_3P_2

Any rational design of a photovoltaic solar cell device rests on the knowledge of energy position of the fundamental absorption edge; the value of the absorption coefficient above it up to 3.5 eV approximately; and the energy factor of reflectance within the same energy range.

The smallest energy bandgap of Zn_3P_2 has been ascribed to indirect transitions with onset at 1.315 eV and the fundamental absorption edge to direct transitions at the gamma point with onset at 1.51 eV, both values at room temperature [1]–[3]. Absorption coefficient of Zn_3P_2 has been found to be relatively high above the fundamental absorption edge, i.e. higher than 10^4 cm^{-1}. The energy factor of reflectance for normal-incident unpolarized light reflected from a single Zn_3P_2 crystal is discussed in [1]. The results of reflectivity for polarized light and the real

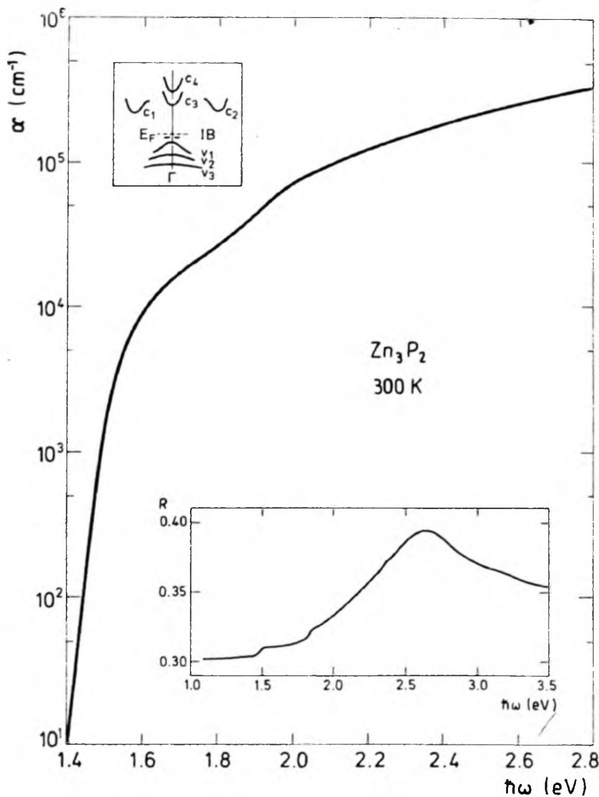

Fig. 1. Experimental data of Zn_3P_2 absorption coefficient and reflectivity factor (lower insert) near the fundamental absorption edge. Upper insert shows the schematic band diagram of Zn_3P_2 from [2]

and imaginary parts of complex dielectric constant of oriented Zn_3P_2 single crystals are presented in [4]. Energy factor of reflectance for thin Zn_3P_2 films is shown in [5]. Standard absorption coefficient and reflectivity spectra of Zn_3P_2 (for unpolarized light) are shown in Fig. 1 together with the schematic band diagram proposed after [2].

Lattice modes of Zn_3P_2 were studied by infrared absorption in [6]. The principal absorption bands lay in 20–25 micrometer waverange and numerous smaller bands were seen and attributed to multiphonon processes. Infrared absorption of single Zn_3P_2 crystals were also studied in [7]. The multiphonon absorption within 0.06–0.11 eV and impurity absorption within 0.5–1.4 eV range have been found. Particularly, the impurity and/or impurity-like levels have been identified at energies of 0.17, 0.26, 0.36, 0.65, 0.87 and 1.28 eV, at 300 K.

3. Electronic properties of Zn_3P_2

Both majority and minority carrier transport properties and their recombination in the bulk and on the surface of semiconductor are of obvious importance to the successful design of any solar cell.

All samples of Zn_3P_2 measured so far have shown p-type conductivity over the temperature range of 80–380 K. The room-temperature resistivity has been usually between 10 and 200 ohm × cm, corresponding to the average value of hole concentration of 10^{21}–10^{22} cm^{-3} and hole mobility of $(10–30)\,10^{-4}$ m^2V^{-1} sec^{-1}. The resistivity of as-grown samples has apparently depended on preparation conditions, ambient atmosphere, and thermal history of the sample. Ionized-impurity scattering at low temperatures and acoustic-phonon scattering at high temperatures have been found as the dominating mechanisms [8], [9]. The surface recombination velocity has been found to dominate over the bulk one. However, the presence of grain boundaries has not appeared to be detrimental to the bulk recombination. The experimentally observed dependence of acceptor concentration on phosphorus pressure [10] suggested phosphorus interstitials to be acting as acceptors. Analysis of the resistivity and Hall-effect measurements in the 4.2–300 K temperature range shown in [11] has resulted in suggestion of two (at least) acceptor levels with energy of 0.035 and 0.6 eV above the valence band.

A minority carrier diffusion length has a great impact upon the solar cell performance and configuration. The diffusion length of electrons in Zn_3P_2 has been estimated by means of several methods to be of the order of a few micrometers. The spectral photoresponse measurements [12], [13], electron-beam induced current method [14], and laser-spot scanning method [15] have been reported.

4. Other properties of Zn_3P_2

The Zn_3P_2 lattice has (up to approx. 1053 K) tetragonal symmetry belonging to the D_{4h}^{15} space group. The dimensions of the unit cell are $a = b = 0.8097$ nm and

$c = 1.145$ nm, and this cell contains 40 atoms. At about 1053 K the tetragonal phase transforms to the cubic one with lattice constant 0.582 nm, and this cell contains 10 atoms. Some information on crystal structure, preparation and the thermodynamic properties of Zn_3P_2 has been given in [16]. A brief discussion of the relationship of bonding to the crystal structure has been published in [5].

Among many semiconductors being investigated actually for application as solar cell devices, only a few meet the requirements of abundance and low cost of fabrication. The power potential of these materials (in GW) based on the known world reserves and a 4-micrometer thick semiconductor layer is very large (more than 10^6 GW) for poly-Si, a-Si and Zn_3P_2; and equal to 10^5 GW for CdS, 400 GW for GaAs, 200 GW for CdTe and 12 GW for InP [17]. Therefore, the practically possible number of semiconductors seems to be limited to the first four ones, with Zn_3P_2 included.

5. Problems with Zn_3P_2

5.1. Doping

Concerning the conductivity type, there are two related phenomena found in Zn_3P_2: only p-type conductivity has been observed and there was impossible to obtain n-type conductivity material in any known way. Both phenomena are, in a general sense, related to defect chemistry in Zn_3P_2. Although the attempt to understand the p-type conductivity mentioned above has been made in [10], this effort ended up with indication of phosphorus interstitials as a source of p-type conductivity, with no detailed analysis of the on-n-type doping problem. The change from p-type to n-type conductivity suggested in [14] to be a result of heating the Mg-Zn_3P_2 Schottky devices seems rather to be caused by the formation of some compounds (e.g., Mg_3P_2) and/or dipoles on the surface (if chemical reaction model of barrier formation is applicable). Magnesium seems to be the only metal that is capable of providing this type of surface reactions (see also below for further discussion). On the other hand, crystal structure of Zn_3P_2 is highly complex (40 atoms per unit cell) and defective. In addition to phosphorus interstitials, the presence of Zn vacancies has been firmly established [16]. Therefore, self-compensation effect is likely to occur in Zn_3P_2. It refers to compensation of any donor impurity due to native defects generated in the crystal lattice. This effect is currently under thorough examinations.

5.2. Surface properties

Zn_3P_2-surface properties and metal-Zn_3P_2 interface reactions are relatively uninvestigated; furthermore they are unusually interesting for the ohmic contact and barrier contact fabrications (see also discussion on doping problem above). More than ten metals were used to prepare the contacts with Zn_3P_2 [18]–[20] and the contact-barrier heights for the metal used did not show simple Schottky-type dependence on metal work-function. Instead, the results correlated quite well with the

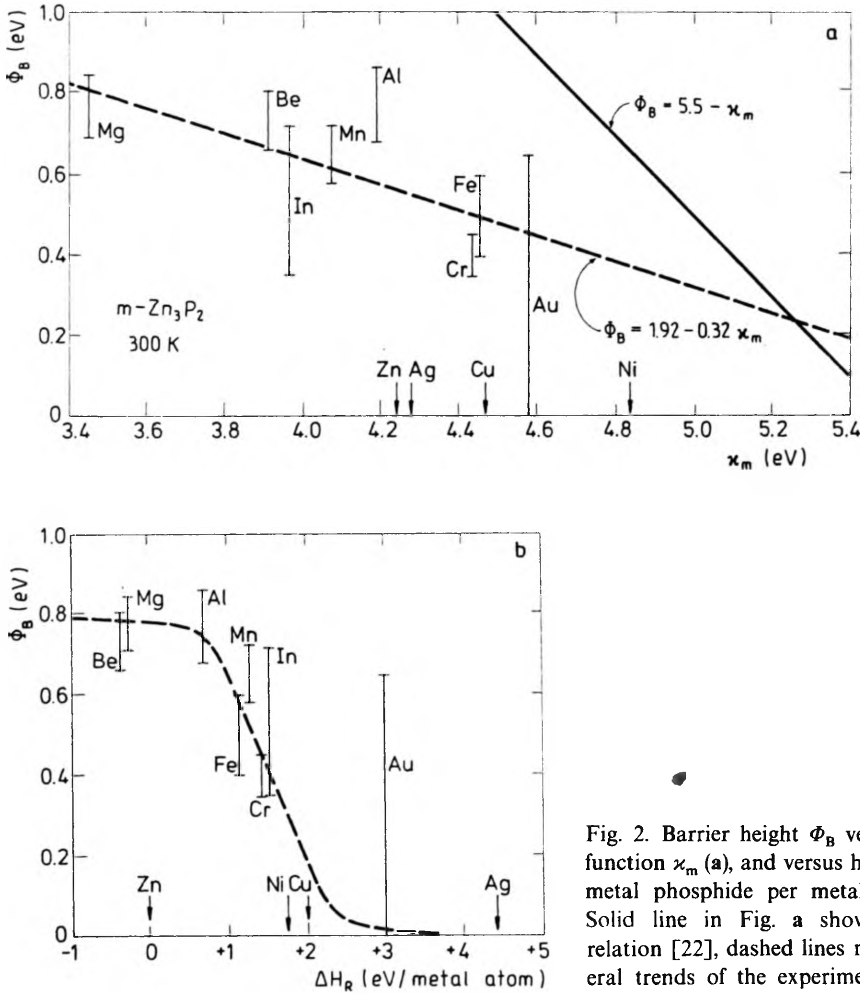

Fig. 2. Barrier height Φ_B versus metal work function $\varkappa_m$ (**a**), and versus heat of reaction of metal phosphide per metal atom ΔH_R (**b**). Solid line in Fig. **a** shows the Schottky relation [22], dashed lines represent the general trends of the experimental results

chemical reaction model proposed in [21] with Mg provided the highest barrier obtainable.

The results of measurements (taken from [19] and from our lab) are presented in Figs. 2**a**, **b**. The barrier height Φ_B measured by various methods (current-voltage and capacitance-voltage characteristics and internal over-the-barrier photoemission spectra) for twelve metal contacts is shown in Fig. 2**a** along with the metal work function. The great scatter of results for In and Au particularly should be noticed. Furthermore, visible difference between the simple Schottky relation [22] shown in Fig. 2**a** as a solid line and the general trend of the experimental results should be underlined. The experimental data can be approximated (according to the model including the surface states effect [23]) linearly and this approximation is shown as dashed line in Fig. 2**a**. Surface state density can be estimated [23] from this dependence. Its value (for the data from Fig. 2**a**) is of the order of $10^{17} m^{-2} eV^{-1}$,

approximately*, which indicates a relatively high influence of the surface states upon the electrical properties of the metal-Zn_3P_2 contacts — within the frame of the model considered.

The barrier height versus heat of reaction of metal phosphide, ΔH_R (per metal atom) of twelve metals with Zn_3P_2 is shown in Fig. **2b**. The results are taken from [19] and from our measurements. The better correlation between the general shape of dependence of Φ_B vs. ΔH_R (dashed line) and the experimental results emerges from this figure then from Fig. 2**a**. It adds strength to the concept of the chemical bonding at the interface metal-zinc phosphide. An important feature of this concept is the occurrence of the maximum value of Φ_B; in this case it is equal to 0.8 eV approximately. Therefore, the metal-Zn_3P_2 junctions under AM1 condition of illumination will not show the open-circuit voltage greater than 0.5 V approximately.

Preparation of a low-resistivity ohmic contact with Zn_3P_2 is still an apparent problem and Ag seems to be the best choice according to [19], [20]; see also Figs. 2**a**, **b**. On the other hand, the long-term stability of Zn_3P_2-based devices are mostly dependent on the surface/interface behaviour. The stability is of a great importance in Mg-Zn_3P_2 Schottky-type devices especially, for Mg_3P_2 (if created) being unstable.

5.3. Photoresponse origin

Thorough studies on photovoltage response of metal-Zn_3P_2 devices [18], [20], [24], [29], [30] showed the negligible effect of recombination centers within the Zn_3P_2 energy gap on the measured spectral characteristics, although the presence of these centers is highly probable (see Sect. 3). They could result in enhanced tunneling and thus in deteriorated conversion performance. In contrast, the study suggests relatively strong impact of surface/interface recombination. Also, the study revealed the space-resolved photovoltage effect, i.e., the strong influence of the light spot position in between the contacts on the sign and value of the photovoltage response. That effect is, in the first approximation: i) related to the two-type-carrier excitations (electrons from impurity levels and/or indirect band-to-band transitions and those from the direct ones); ii) influenced by the photostatic effect in high-resistivity samples, and iii) caused by the high surface recombination, as well. This problem has recently been discussed thoroughly in [30].

6. Zn_3P_2-based solar cell devices

6.1. Theoretical estimations

The computations have been made of photon collection efficiency (PCE), carrier collection efficiency (CCE), short-circuit current (j_{sc}) and total conversion efficiency (TCE), of the prototype Zn_3P_2-based solar cell devices [25]–[27]. Results of these calculations, together with discussion of quantum efficiency (QE) of photo-genera-

* The value of $8 \times 10^{16} m^{-2} eV^{-1}$ has recently been obtained [28].

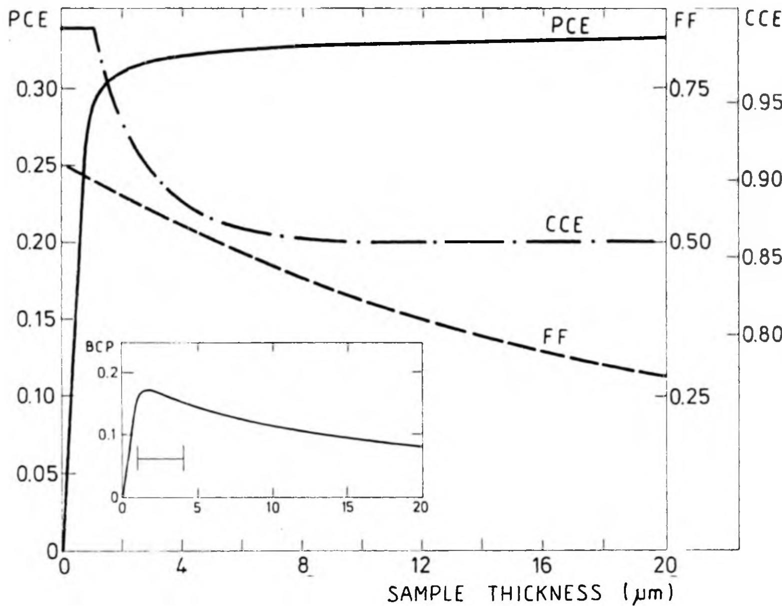

Fig. 3. Photon-collection and carrier-collection efficiencies versus sample thickness, computed for bare-surface front-wall configuration Zn_3P_2-based solar cell. Fill factor computed by taking into account the contact resistivity equal to 10 ohms is also shown as a function of thickness. BCP factor (see the text) versus sample thickness is shown as an insert

tion processes in Zn_3P_2 are extensively analyzed in [25], [26]. The fill-factor (FF) of the prototype devices has been computed in [27] by taking into account the generation-recombination processes in the field-in-built region as a dominating mechanism in carrier transport through the junctions and the series resistivity of the devices as caused by the Zn_3P_2 resistivity only, with contact resistivity being negligible.

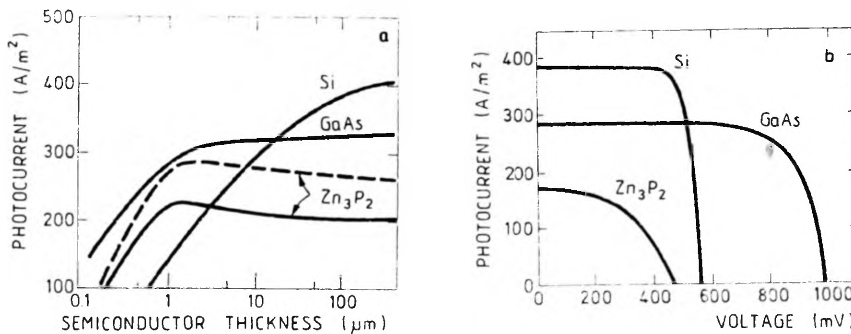

Fig. 4. Peak value of photocurrent (short-circuit current density) computed in a function of the semiconductor base thickness under AM1 illumination condition (**a**), and the photocurrent-versus-voltage experimental characteristics (**b**) taken for Si and GaAs from [32] and for Zn_3P_2 from [27]

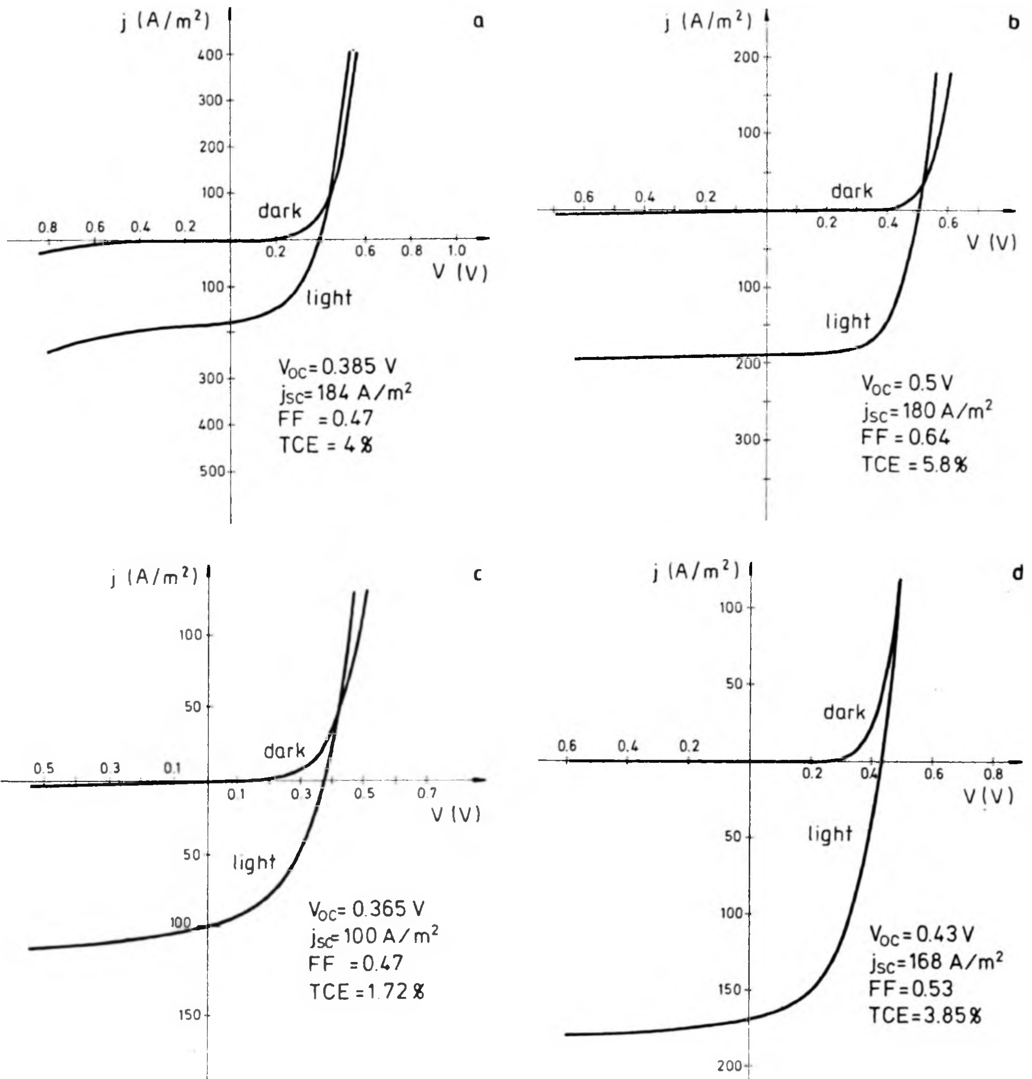

All the fundamental parameters of the solar cell devices are thickness-dependent. The plots of PCE, CCE and FF versus Zn_3P_2 thickness are shown in Fig. 3. Their product, called here the best-compromized parameters (BCP) factor, is shown there as an insert. The BCP-versus-thickness plot clearly indicates that the most appropriate thickness of Zn_3P_2 sample for solar energy conversion is within the range of 1.5–4 micrometers.

Looss figures and output data (taken from [27]) of four theoretically considered Zn_3P_2-based devices are listed in the Table, including the opaque-metal grid (OMG) and transparent-metal film (TMF) Schottky-type metal-semiconductor junctions, p-n homojunction and p-n heterojunction. Results for bare Zn_3P_2 sample are also shown for comparison. The computations have been made under AM1.5 conditions of illumination (density of power equal to 832 Wm^{-2}).

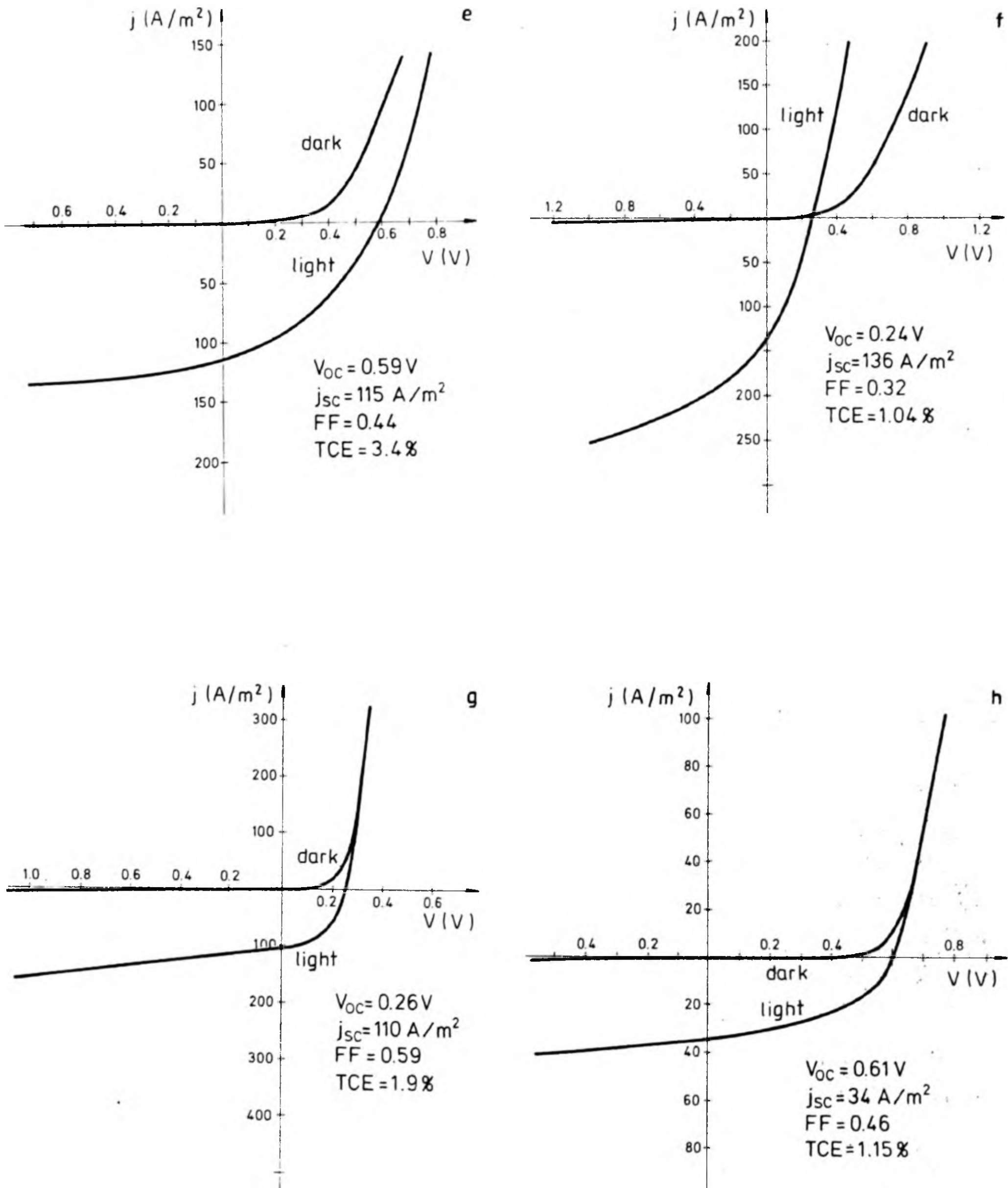

Fig. 5. Current voltage characteristics of prototype Zn_3P_2-based solar cells: **a** – OMG Mg-Zn_3P_2 device with no AR coating, after [34]; **b** – OMG Mg-Zn_3P_2 device with 80 nm SiO AR coating, after [36]; **c** – TMF 15 nm Mg-Zn_3P_2 device with 500 nm SiO AR coating, after [36]; **d** – TMF 10 nm Mg-Zn_3P_2 device with 70 nm ZnO AR coating, after [39]; **e** – n-p Zn_3P_2 quasi-homojunction device with no AR coating, after [42]: **f** – n-p ITO-Zn_3P_2 heterojunction device with no AR coating, after [49]; **g** – n-p ZnO-Zn_3P_2 heterojunction device with no AR coating, after [50]; **h** – n-p ZnSe-Zn_3P_2 heterojunction device with no AR coating, after [43]. "Light" curves in Fig. **a**–**e** were measured under AM1 and these curves in Figs. **g**, **h** under AM1.5 conditions of illumination. Curves in Fig. **f** were measured under 1000 W/m^2 illumination density

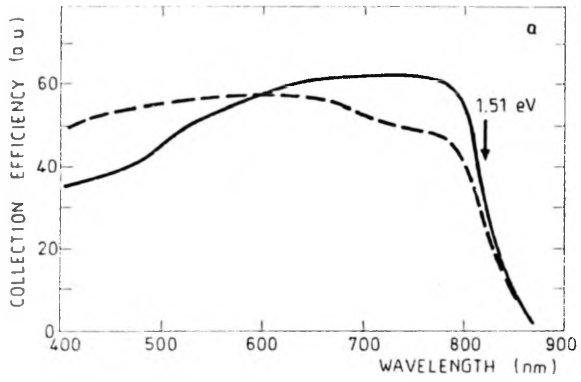
a
COLLECTION EFFICIENCY (a.u.)
WAVELENGTH (nm)
1.51 eV
0
20
40
60
400
500
600
700
800
900

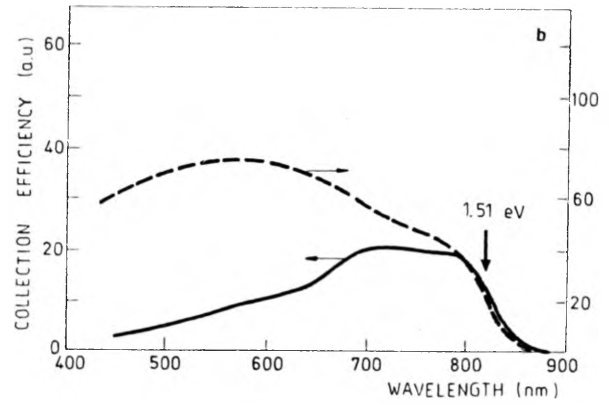
b
COLLECTION EFFICIENCY (a.u)
WAVELENGTH (nm)
1.51 eV
0
20
40
60
100
60
20
400
500
600
700
800
900

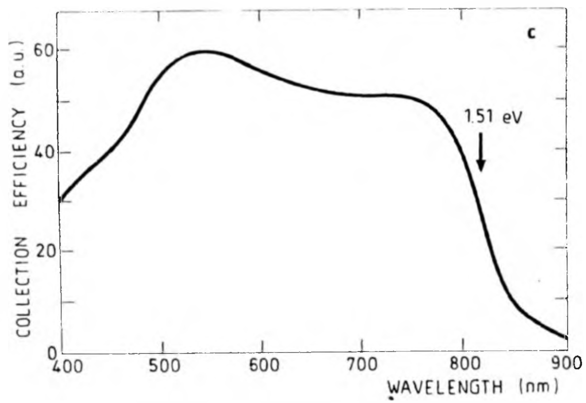
c
COLLECTION EFFICIENCY (a.u.)
WAVELENGTH (nm)
1.51 eV
0
20
40
60
400
500
600
700
800
900

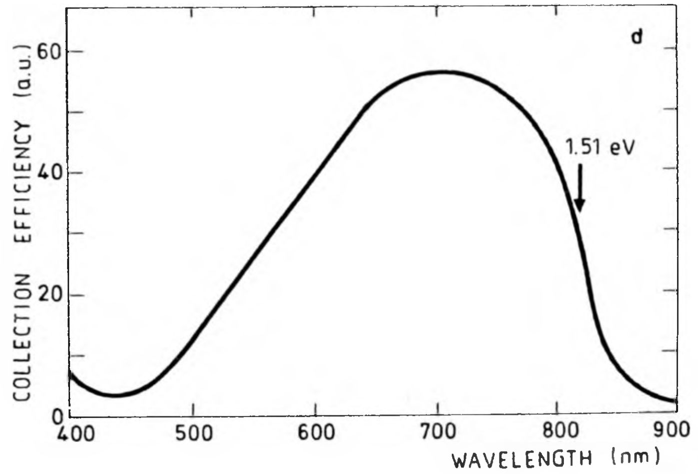
d
COLLECTION EFFICIENCY (a.u.)
WAVELENGTH (nm)
1.51 eV
0
20
40
60
400
500
600
700
800
900

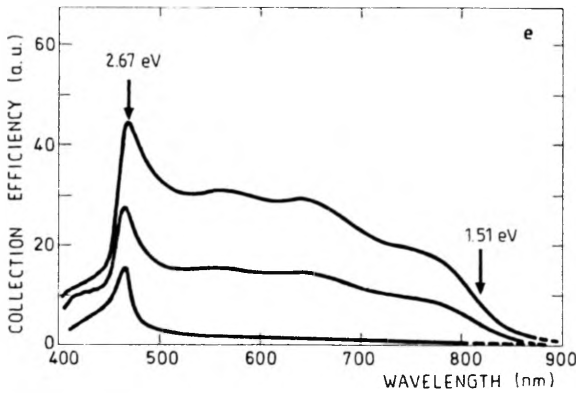

Fig. 6. Overall collection efficiency (photoresponse measured in output-current mode) of prototype Zn_3P_2-based solar cells: **a** – OMG Mg-Zn_3P_2 device with no AR coating (dashed line), after [34], and that with 93 nm SiO coating (solid line), after [36], (both under AM1 conditions of illumination). **b** – TMF 10 nm Mg-Zn_3P_2 device with 70 nm ZnO AR coating (dashed line), after [36], and n-p Zn_3P_2 quasi-homojunction device with no AR coating (solid line), after [42], (both the curves under AM1 conditions of illumination). **c** – n-p ITO-Zn_3P_2 heterojunction device with no AR coating, under 1000 W/m^2 illumination, after [49]. **d** – n-p ZnO-Zn_3P_2 heterojunction device with no AR coating, under AM1.5 conditions of illumination, after [50]. **e** – n-p ZnSe-Zn_3P_2 heterojunction device with no AR coating, after [43], (curves were measured under AM1.5 light conditions and voltage bias of 2 V, 1 V and 0; from top to bottom, respectively)

The maximum photocurrent (short-circuit current density) computed for Zn_3P_2 solar cell as a function of Zn_3P_2 thickness is shown in Fig. 4**a** together with the data taken from [31] for Si- and GaAs-based solar cells. The lower curve for Zn_3P_2-based devices is computed for bare surface (no antireflection coating) semiconductor; the upper one shows the potentiality of devices with the best multilayer antireflection coating having reflectivity factor of 5% approximately. The computations have been done under AM1 conditions of illumination (power density equal to 930 Wm^{-2}).

Figure 4**b** shows the experimental current-voltage characteristics of three prototype devices under AM1.5 conditions. This figure reveals the place of the prototype Zn_3P_2-based solar cells in comparison to the best ones fabricated on the

Loss figures and output data of Zn_3P_2-based solar cells under AM1.5 illumination integrated over 0–∞ waverange, with AR coating, after [27]

Type of device	Total optical losses [%]	Total electrical losses [%]	Short-circuit current [A/m^2]	TCE [%]
OMG Schottky junction	76.9	10.7	137	12.4
TMF Schottky junction	87.7	5.1	73.5	7.2
p-n homojunction	71.5	13.3	165	15.2
p-n heterojunction	69.6	14.2	181	16.2
Bare Zn_3P_2	68*	14.9	190	17.1

* value of ≃ 60% is the lowest number of optical losses assuming the best multilayer AR coating with R ≃ 5%

base of Si and GaAs. The data for the Si- and GaAs-based devices have been taken from [32] and for the Zn_3P_2-based one from [27].

Potentiality of Zn_3P_2-based solar cells shown in Fig. 4**a** is comparable to that of GaAs-based devices. Reality exposed in Fig. 4**b** does not match the potentiality, unfortunately, for some reasons that will be discussed in details below.

6.2. Metal-Zn_3P_2 devices

Both the OMG and TMF Schottky-type metal-Zn_3P_2 devices have been fabricated and tested. Among all the metals used, Mg has been found to form (statistically) the highest (0.8 eV) potential barrier with Zn_3P_2 (see above) although the other metals have also been examined.

The OMG prototype solar cells have been made of both the polycrystalline bulk samples and the polycrystalline thin film specimens [33]–[36]. The best parameters of the OMG cells have been to date presented in [34], [36]. By using magnesium grid pattern whose line separation was approximately twice the minority carrier diffusion length (and with no antireflection coating) an active area current density as high as $j_{sc} = 183$ A/m^2 was obtained with V_{oc} slightly lower than 0.4 V and TCE = 1.5%. For the same type OMG devices with AR coating the best parameters obtained are: $j_{sc} = 190$ A/m^2, $V_{oc} = 0.5$ V and TCE up to 6% [36]. The experimental current-voltage and spectral characteristics of the best OMG-type devices without and with AR coating taken from [34] and [36], respectively, are shown in Figs. 5**a**, **b** and 6**a**, respectively. Dark and light I–V curves intersect for these devices which can suggest a change of the transport mechanism of carriers across the junction under illumination. The reasonably flat spectral response of the devices at short wavelengths can indicate negligible losses due to surface recombination. Schematic Schottky-type equilibrium band diagram of Mg-Zn_3P_2 structure is shown in Fig. 7**a**. The band-bending region width is estimated (from simple estimation for parabolic barrier) to be 1.75 μm.

The TMF prototype solar cells have been fabricated by means of dc sputtering or PVD thermal evaporation of thin (10–15 nm) magnesium layer on the top of both the polycrystalline bulk samples and the polycrystalline thin film specimens [29], [35]–[39]. The best parameters obtained for the TMF devices have been to date presented in [38], [39] for devices with 70 nm ZnS AR coating. Short-circuit current up to 178 A/m^2 and V_{oc} as high as 0.51 V have been attained with TCE around 4–5%. The experimental current-voltage and spectral characteristics of the best TMF-type devices (which differ in the thickness of both the Mg film and the AR coating) taken from [36], [39] are shown in Figs. 5**c**, **d** and Fig. 6**b**, respectively. High optical losses due to reflection from and absorption within the Mg film limit the output photo-current. The relatively low values of fill factor (not exceeding 0.6) are due mainly to the high diode factor ($\simeq$ 2) connected presumably with the space-charge recombination mechanism. The V_{oc} value, on the other hand, is limited by the $\simeq 0.8$ eV maximum barrier height of the metal-Zn_3P_2 junction (see also above). The collection efficiency is fairly constant in the short-wavelength range. The

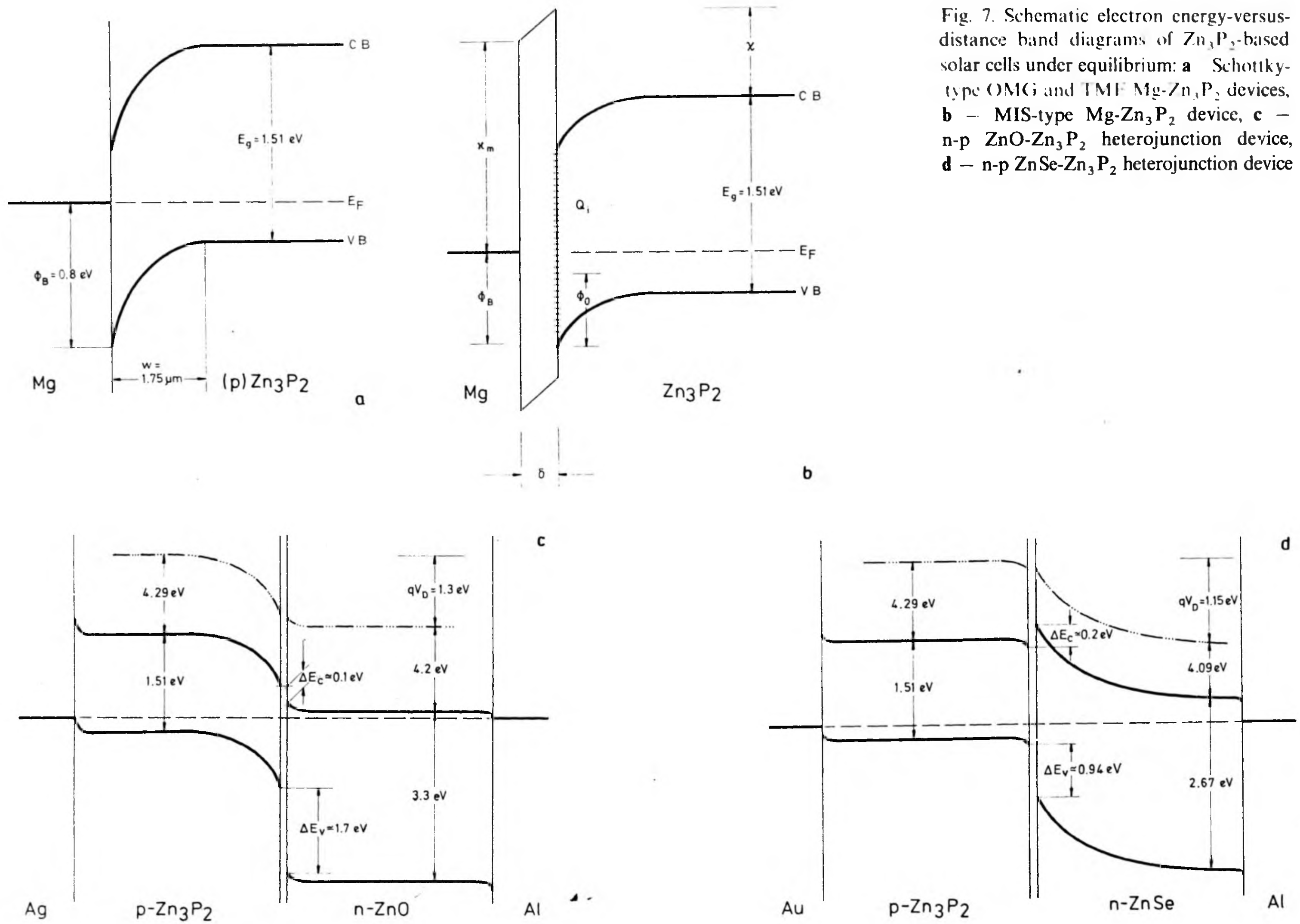

Fig. 7. Schematic electron energy-versus-distance band diagrams of Zn_3P_2-based solar cells under equilibrium: **a** – Schottky-type OMG and TMF Mg-Zn_3P_2 devices, **b** – MIS-type Mg-Zn_3P_2 device, **c** – n-p ZnO-Zn_3P_2 heterojunction device, **d** – n-p $ZnSe$-Zn_3P_2 heterojunction device

comparison between the devices made of the large-grain polycrystalline bulk samples and these made of the small-grain thin films shows that the grain boundaries in the large-area devices do not seriously compromise the device performance. However, we should recall that the grain-boundaries detrimental effect is always decreased under illumination [40].

Although n-type Zn_3P_2 has never been prepared in any direct way and in any form (bulk or thin-film specimen) Zn_3P_2 p-n homojunction formation has been reported [14], [41] in the TMF Mg-Zn_3P_2 devices after their heating for a few hours at 75–100°C. The evidences presented in these papers to add strength to suggestion of the p-n junction creation can, however, be (in part, at least) ascribed to the concept of the dipole-layer formation (see also Sect 5). This metal-dipole layer-semiconductor structure is, in general sense, similar to the MIS one shown in Fig. 7 **b**. The formation of the interface between Mg and Zn_3P_2 and particularly its thickness δ is obviously time- and temperature-dependent as well. Nevertheless, the experimental current-voltage and spectral characteristics of nominally p-n Zn_3P_2 homojunction devices are shown in Fig. 5**e** and Fig. 6**b**, respectively, after [42]. The values of j_{sc} up to 153 A/m^2 and these of V_{oc} as high as 0.57 V have been measured under AM1 illumination conditions. The FF value in the range of 0.4–0.47 has been found giving TCE values up to 3.7%. Therefore, the overall performance of the TMF Mg-Zn_3P_2 devices is lower after heating, i.e., after suggested transformation into p-n homojunction devices. Particularly, the decrease in j_{sc} values and the increase in V_{oc} values strengthens the concept of dipole layer formation rather than the suggestion of p-n junction creation [14], [41]. Nevertheless, the formation of n-on-p junction by heating the Mg-Zn_3P_2 structure is a continuously open question.

6.3. Heterojunctions n-p devices

The highest value of the open-circuit voltage in the prototype OMG and TMF Mg-Zn_3P_2 devices achieved to date (in TMF solar cells) has been $V_{oc} \simeq 0.5$ V. This relatively low value is, however, equal to the upper limit of V_{oc} estimated for Mg-Zn_3P_2 devices, approximately (see above). For this reason, the search for an appropriate heterojunction partner for Zn_3P_2 has been carried out. The heterojunction-partner semiconductor with $E_g > E_g(Zn_3P_2)$ is improving the V_{oc}, while that with $E_g < E_g(Zn_3P_2)$ is giving the higher j_{sc} values; assuming that the generation and collection of minority carriers are taking place equally in both the materials, approximately. The following parameters are usually instrumental in the material selection for heterojunctions: energy bandgap; electron affinity, lattice constant and thermal expansion coefficient.

Both isostructure and anisostructure heterojunctions with Zn_3P_2 have been investigated (see [43]–[45], for short review) including II–V binary and ternary compounds such as $(Cd_xZn_{1-x})_3P_2$ and Mg_3P_2, ITO, and II–VI binary and ternary compounds such as CdO, CdS, ZnO, ZnS, ZnSe and $Zn_xCd_{1-x}S$.

II–V binary compounds and their solid solutions (ternary mixed crystals) are apparent isostructure partners for Zn_3P_2. However, all (but one, Mg_3P_2) have the

energy gap smaller than that of Zn_3P_2. The E_g value of Mg_3P_2 is (direct bandgap) 2.5 eV, approximately, but the material is highly unstable in air [46]. Looking for the lower bandgap n-type material to improve j_{sc} output, it appears that only Cd_3P_2 (either $E_g = 0.53$ eV [47] or 0.56 eV [48] at 300 K) is available. It can produce ternary mixed crystals Cd_3P_2-Zn_3P_2 possessing the n-type conductivity together with the appropriate energy bandgap [36], [48]. The (n)$Cd_{3x}Zn_{3-3x}P_2$-(p)Zn_3P_2 heterojunctions with $x > 0.5$ were investigated and the p-n barrier height was found to be 0.77 eV [44]. However, low values of both the V_{oc} and j_{sc} were measured and no further work was performed.

Heavily doped n-type and optically transparent ($E_g = 3.6$ eV [55]) *indium-tin oxide* (*ITO*) seems to be an attractive partner to any p-type semiconductor. ITO-on-Zn_3P_2 heterojunction devices have been fabricated by rf sputter deposition of about 300 nm thick ITO (having $\simeq 90\%$ of optical transmission) onto sputter cleaned Zn_3P_2:Ag [49]. The V_{oc} values of 0.24–0.32 V and j_{sc} values of 130–260 A/m^2 have been reported with total conversion efficiency up to 1.1% under 1000 W/m^2 illumination density. One should note the unbelievably high density (260 A/m^2) of photocurrent listed in [49]. The experimental current-voltage and spectral characteristics of ITO-Zn_3P_2 prototype solar cell are shown in Fig. 5**f** and Fig. 6**c**, respectively, after [49]. The shape of the I–V curves has been ascribed in [49] to the tunneling mode as dominating transport mechanism. The very low value of FF has been attributed to high series resistance and large diode factor. The first reason is the hardly expected one in ITO-contained devices. The relatively low V_{oc} might come from carrier recombination by the interface states and/or by Zn_3P_2 surface states. The last suggestion is strengthened by the shape of the spectral characteristic shown in Fig. 6**c**, in which the high drop of protocurrent in blue region is well visible.

II–VI binary compounds such as thoroughly studied CdS, ZnS, ZnO and ZnSe appear attractive candidates because (among other things) a wide variety of preparation techniques. Furthermore, they satisfy the requirements mentioned above quite well (see, e.g. [43], for short review). A natural partner for any zinc compound is zinc oxide (common cation) and (n)ZnO-(p)Zn_3P_2 heterojunction solar cells were prepared and described in [50], [51]. The 100 nm thick low resistivity ZnO film was dc sputter deposited on sputter cleaned silver-doped polycrystalline Zn_3P_2 wafers. The maximum values of $V_{oc} = 0.38$ V and of $j_{sc} = 46$ A/m^2 were measured under 850 W/m^2 illumination density (somewhere in between AM1 and AM1.5 conditions) on as-prepared devices. Low j_{sc} value is due principally to the high series resistance of ZnO and in order to reduce that resistance and to provide good ohmic contact to ZnO film the aluminium (100 nm thick) layer dots were deposited by PVD-thermal evaporation. The experimental current-voltage and spectral characteristics of the best example of such a device are shown in Fig. 5**g** and Fig. 6**d**, respectively. The best value (corrected for an active area) of $j_{sc} = 110$ A/m^2 was obtained, however, a long with V_{oc} decreasing to $V_{oc} = 0.26$ V. Fill factor up to 0.586 and TCE as high as 1.9% was found. Well visible maximum of collection efficiency arises from the p-side of heterojunction. The next peak (from ZnO region) is expected in the blue region (below 375 nm) for high ZnO energy bandgap ($E_g = 3.3$ eV is reported in [52]).

Between these peaks there is a rapid fall-off, suggesting strong recombination at the interface. The schematic equilibrium band diagram of n-p ZnO-Zn_3P_2 heterojunction is shown in Fig. 7**c**. It has been constructed using the known values of electron affinities and energy band gaps [43]. Note the differences between the model shown in Fig. 7**c** and the one presented in [50] as Fig. 4. Diffusion voltage as high as $V_D = 1.3$ V is deduced from the diagram. It appears likely that the interface states are highly instrumental in decreasing the V_{oc} with reference to the relatively high V_D value.

Two others II–VI compounds, namely n-type CdS ($E_g = 2.42$ eV) and n-type ZnS ($E_g = 3.6$ eV), have provided even noticeably worse results than those for ZnO [43], [44]. High leakage current and low values of both the V_D and V_{oc} were found.

Looking for solar-spectrum transparent and reasonably low electron affinity material, n-type thin ZnSe film ($E_g = 2.67$ eV [56] at 300 K) appears to be a promising common-cation partner. The (n)ZnSe:Ga-(p)Zn_3P_2 heterojunctions were prepared, essentially by the thin-film technique described in [43], [56]. The experimental results of current-voltage and spectral characteristics measured under AM1.5 illumination conditions are shown in Fig. 5**h** and Fig. 6**e**, respectively. The values of V_{oc} as high as 0.84 V and j_{sc} up to 37.5 A/m^2 were obtained. Fill factor slightly lower than 0.5 along with the TCE value up to 1.8% were found. Low value of j_{sc} (in comparison with the estimated one listed in the Table, particularly) is (most probably) the result of the high resistivity of the ZnSe film and then high series resistance of the device. Equilibrium schematic energy band diagram of (n)ZnSe-(p)Zn_3P_2 heterojunction is shown in Fig. 7**d** after [43]. Taking the known values of parameters of both the semiconductors [43], the value of $V_D = 1.15$ V is deduced from the diagram, being in a reasonable reference to the measured V_{oc} values (much better than for ZnO-Zn_3P_2 heterojunction – see above). As it results from Fig. 7**d**, almost the entire built-in-field region is hidden inside the n-type semiconductor. This is in favour of higher photo-current output from ZnSe than that from Zn_3P_2 as shown in Fig. 6**e** (note that this situation is quite different than that in the case of both the ITO-Zn_3P_2 and the ZnO-Zn_3P_2 heterojunctions). Carrier collection in Zn_3P_2 is then affected by generation-recombination mechanism in the bulk with almost no barrier electric field involved. At least, two order of manitude higher donor concentration in ZnSe is needed to optimise the heterojunction [43]. However, obtaining of highly doped n-type ZnSe films has been an apparent problem [53], [54], [56]. The impact of the recombination at the heterojunction interface upon the j_{sc} value is presumably high as well.

7. Final conclusions

Zn_3P_2 has become one of the promising semiconductors for applications in photovoltaic solar energy conversion. Both the values of the direct energy bandgap and the diffusion length of electrons promote the reasonably high energy conversion efficiency factor. Also, both Zn and P are abundant and inexpensive. Prototype Zn_3P_2-based solar cell devices in various configurations have been recently

fabricated and tested. It has been shown that the prototype devices meet roughly the design calculation results and that the value of TCE about 6% can be accomplished relatively easily. After some optimization procedure, TCE up to 16% can be achieved [27] strengthening the need to promote further investigations of both the fundamental properties of Zn_3P_2 and the electronic performance of Zn_3P_2-based photovoltaic thin film devices.

Investigations of the nature of the photoelectric properties of Zn_3P_2 and Zn_3P_2-based devices still leave many unaswered questions. One of it is the presence of deep levels within Zn_3P_2 bandgap since they are probably responsible for the carrier tunneling under intense illuminations, eventually resulting in low V_{oc} values. Also, the surface properties of Zn_3P_2 are of an unusually great interest, being furthermore closely related to the device performance.

As far as prototype solar cells are concerned, all the empirical results suggest a dominant role of the interface (between Zn_3P_2 and its partner to form a potential barrier). An exception is p-n homojunction device and one of the evident courses of action is to fabricate the p-n junction in Zn_3P_2. However, the problem of the appropriate doping of Zn_3P_2 to convert it into n-type material has to be solved above all. On the other hand, magnesium appears to be the only metal that is capable of providing beneficial interface reaction to Zn_3P_2. OMG and TMF Mg-Zn_3P_2 junctions are therefore the reasonably good configurations for solar cell applications, providing that suitable fabrication procedure is used. The low V_{oc} value limited by the potential barrier height of Mg-Zn_3P_2 structure to $V_{oc} \simeq 0.5$ V is however a distinct disadvantage of the Mg-Zn_3P_2 devices.

Heterojunction-type Zn_3P_2-based solar cells are of a great interest having a clear advantage of possibility to obtain very high V_{oc} in case of wide-bandgap partner material. Such a heterojunction partner can also serve as an optical window/antireflection coating. ZnSe appears to be very appropriate semiconductor on condition that the successful high ($\simeq 10^{21} m^{-3}$) donor doping will be assured, and electronic properties of the metalurgical interface ZnSe-Zn_3P_2 will be improved, as well.

In any case of configuration, all-thin-film solar cell structures are required to achieve the best conversion efficiency and the ultimate economic goal for a large -scale electricity generation.

Acknowledgements – The fruitfull discussions with Dr Dr M. Bhushan, A. W. Catalano, and J. D. Meakin from IEC, University of Delaware; and Dr Dr N. Mirowska, J. Misiewicz and K. Nauka from IP, Technical University of Wrocław, are gratefully acknowledged.

References

[1] Pawlikowski J. M., Misiewicz J., Mirowska N., J. Phys. Chem. Solids **40** (1979), 1027.
[2] Pawlikowski J. M., J. Appl. Phys. **53** (1982), 3639.
[3] Pawlikowski J. M., Phys. Rev. B **26** (1982), 4711.
[4] Misiewicz J., Wróbel J., Jezierski K., J. Phys. C: Solid State Phys. **17** (1984), 3091.
[5] Fagen E. A., J. Appl. Phys. **50** (1979), 6505.

[6] Radautzan S. I., Syrbu N. N., Nebola I. I., Volodina V. I., Sov. Solid State Phys. **19** (1977), 1290.
[7] Misiewicz J., Sujak-Cyrul B., Bartczak A., Solid State Commun. **58** (1986), 677.
[8] Wang F.-C., Fahrenbruch A. L., Bube R. H., *Proc. 15th IEEE Photovoltaic Specialists Conf.*, Orlando 1981, p. 1265.
[9] Wang F.-C., Fahrenbruch A. L., Bube R. H., J. Electron. Mater. **11** (1982), 75.
[10] Catalano A. W., Hall R. B., J. Phys. Chem. Solids **41** (1980), 635.
[11] Sieranski K., Szatkowski J., Phys. Status Solidi (a) **94** (1986), K133.
[12] Convers Wyeth N., Catalano A. W., J. Appl. Phys. **50** (1979), 1403.
[13] Nauka K., Misiewicz J., Phys. Status Solidi (b) **65** (1981), K95.
[14] Catalano A. W., Bhushan M., Appl. Phys. Lett. **37** (1980), 567.
[15] Catalano A. W., Masi V. J., Convers Wyeth N., *Proc. 2nd Photovoltaic Solar Energy Conf.*, Berlin 1979, p. 440.
[16] Arushanov E. K., Prog. Crystal Growth Charact. **3** (1981), 211.
[17] Dalal V. L., Baron B. N., Russel T. W. F., *Proc. Meeting of Amer. Section of Intern. Solar Energy Soc.*, June 2–6, Phoenix 1980.
[18] Pawlikowski J. M., Mirowska N., Becla P., Królicki F., Solid State Electron. **23** (1980), 755.
[19] Convers Wyeth N., Catalano A. W., J. Appl. Phys. **51** (1980), 2286.
[20] Mirowska N., Ph. D. Thesis, Technical University of Wrocław, 1984, unpublished.
[21] Brillson L. J., Thin Solid Films **89** (1982), 461.
[22] Schottky, W., Z. Phys. **113** (1939), 367; **118** (1942), 539.
[23] Cowley A. M., Sze S. M., J. Appl. Phys. **36** (1965), 3212.
[24] Mirowska N., Misiewicz J., Nauka K., Pawlikowski J. M., Acta Phys. Pol. A **60** (1981), 231.
[25] Pawlikowski J. M., Opt. Appl. **15** (1985), 3.
[26] Pawlikowski J. M., *Proc. Intern. Conf. Physics and Technology of Compensated Semiconductors*, Madras, Febr. 20–23, 1985, Vol. 1, p. 97.
[27] Pawlikowski J. M., Electron Technology **19** (1986), 75.
[28] Szatkowski J., Sierański K., Solid State Electron. **31** (1988), 257.
[29] Mirowska N., Szatkowski J., Gumienny Z., Infrared Phys. **28** (1988), 97.
[30] Mirowska N., Hafez A. M., Pawlikowski J. M., submitted for publication.
[31] Fan J. C. C., Technology Rev. **80** (1978), 1.
[32] Walker D. H., Statler, R. L., Solar Cells **17** (1986), 309.
[33] Catalano A. W., Masi J. V., Convers Wyeth N., *Proc. 2nd E. C. Photovoltaic Solar Energy Conf.*, Berlin 1979 (Ed. Riedel, Dordrecht, Holland, 1979), p. 440.
[34] Catalano A. W., Bhushan M., Convers Wyeth N., *Proc. 14th IEEE Photovoltaic Specialists Conf.*, San Diego 1980, p. 641.
[35] Misiewicz J., Szatkowski J., Mirowska N., Jezierski K., Gumienny Z., Królicki F., Acta Phys. Pol. A **69** (1986), 1131.
[36] Catalano A. W., Dalal V., Devaney W. E., Fagen E. A., Hall R. B., Masi J. V., Warfield G., Convers Wyeth N., *Final Report* (under contract EX-76-C-01-2460) Institute of Energy Conversion, University of Delaware 1978, unpublished.
[37] Bhushan M., Catalano A. W., *Proc. 15th IEEE Photovoltaic Specialists Conf.*, Orlando 1981, p. 1261.
[38] Bhushan M., Catalano A. W., Appl. Phys. Lett. **38** (1981), 39.
[39] Bhushan M., Appl. Phys. Lett. **40** (1982), 51.
[40] Pawlikowski J. M., Thin Solid Films, in press.
[41] Bhushan M., J. Appl. Phys. **53** (1982), 514.
[42] Bhushan M., Pawlikowski J. M., Pereyra I., *Proc. 161 Meeting Electrochem. Soc.*, Montreal 1982, Vol. **82-8**, p. 505.
[43] Bhushan M., Pawlikowski J. M., Electron Technology **20** (1987).
[44] Bhushan M. et al., *Final Report* (under SERI subcontract XR-9-8062-1) Institute of Energy Conversion, University of Delaware 1982, unpublished.
[45] Wang F.-C., Ph. D. Thesis, Stanford University, 1982, unpublished.
[46] Catalano A. W., Thin Solid Films **83** (1981), L141.

[47] GELTEN M. J., van LIESHOUT A., van ES C. M., BLOM F. A. P., J. Phys. C: Solid State Phys. **11** (1978), 227.
[48] PAWLIKOWSKI J. M., J. Phys. C: Solid-State Phys. **18** (1985), 5605.
[49] SUDA T., KOBAYASHI M., KUROYANAGI A., KURITA S., Jpn J. Appl. Phys. **21**, Suppl. 2 (1982), 63.
[50] NAYAR P. S., CATALANO A. W., Appl. Phys. Lett. **39** (1981), 105.
[51] NAYAR P. S., J. Appl. Phys. **53** (1982), 1069.
[52] DEVALD P., Bell System Techn. J. **39** (1960), 815.
[53] PAWLIKOWSKI J. M., *Proc. Int. Conf. Physics and Technology of Compens. Semicond*, Madras 1985, Vol. 1, p. 105.
[54] SKUDLARSKI K., Jr, PAWLIKOWSKI J. M., Solid State Commun. **60** (1986), 111.
[55] HAINES W. G., BUBE R. H., J. Appl. Phys. **49** (1978), 304.
[56] PAWLIKOWSKI, J. M., Thin Solid Films **127** (1985), 9.

Received May 4, 1988

Солнечные батареи на базе Zn_3P_2

Представлен обзор актуального состояния исследований солнечных батарей на базе Zn_3P_2. Настоящая работа содержит краткое описание основных свойств Zn_3P_2, обсуждение некоторых технологических проблем, а также теоретическую оценку параметров солнечных батарей с Zn_3P_2. Обсуждены также самые лучшие достижения прототипных батарей в конфигурации соединения Шотки (OMG и TMF) и гетеросоединения.